THE JOURNAL OF PHYSICAL CHEMISTRY Letters

Letter

pubs.acs.org/JPCL

Design and Tailoring of a Three-Dimensional TiO_2–Graphene–Carbon Nanotube Nanocomposite for Fast Lithium Storage

Laifa Shen,[†,‡] Xiaogang Zhang,*[,†] Hongsen Li,[†] Changzhou Yuan,[†] and Guozhong Cao[‡]

[†]College of Material Science & Engineering, Nanjing University of Aeronautics and Astronautics, Nanjing, 210016, People's Republic of China

[‡]Department of Materials Science and Engineering, University of Washington, Seattle, Washington 98195, United States

Supporting Information

ABSTRACT: Nanocrystalline TiO_2 grown on conducting graphene nanosheets (GNS) and multiwalled carbon nanotubes (CNTs) via a solution-based method to form a three-dimensional (3D) hierarchical structure for fast lithium storage. CNTs in the unique hybrid nanostructure not only prevent the restacking of GNS to increase the basal spacing between graphene sheets but also provides an additional electron-transport path besides the graphene layer underneath of TiO_2 nanomaterials, increasing the electrolyte/electrode contact area and facilitating transportation of the electrolyte ion and electron into the inner region of the electrode. Such a 3D TiO_2–GNS–CNT nanocomposite had a large specific surface area of 291.2 m^2 g^{-1} and exhibited ultrahigh rate capability and good cycling properties at high rates.

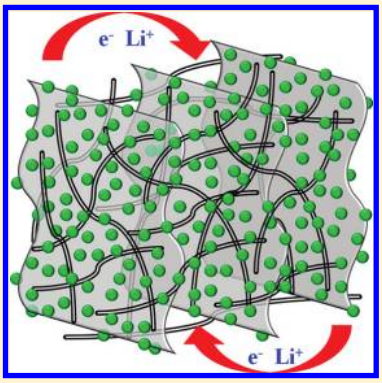

SECTION: Energy Conversion and Storage

Carbonaceous materials used as anodes in commercial lithium ion batteries (LIBs) have slow Li ion diffusion and increased resistance at the electrode/electrolyte interface at high rates, which fails to meet the fast-growing requirements of high-power LIBs.[1,2] Also, the commercial LIBs cannot satisfactorily meet the safety requirements in the future practical applications.[3−5] The anatase TiO_2 has become a highly promising anode material for LIBs. The titanium dioxide offers a great improvement in safety due to its high lithium insertion/deinsertion potential at about 1.7 V versus Li^+/Li and thereby is inherently safe by avoiding Li electroplating. Furthermore, the TiO_2 has high reversible capacity and low volume expansion (3−4%) during lithium ion insertion/deinsertion, leading to enhanced structural stability and a longer cycle life.[6−9]

However, the poor conductivity of TiO_2 greatly results in the poor rate capability and great degradation of capacity upon prolonged cycling, which brings difficulties for high-power LIBs applications.[10,11] Considerable efforts have been made to overcome the electronic and ionic transport limitations to improve the electrochemical performance. Extensive work has focused on tailoring the particle size of TiO_2 to reduce both the ionic and electronic transporting paths[1,12,13] and coat the TiO_2 particles with an electron-conducting layer.[7,9,14,15] The hybrid nanostructure electrode materials with conductive additive nanophases effectively overcome the electronic and ionic transport limitations, thus resulting in excellent lithium storage performance at a high rate.[16] Recently, Cao et al. synthesized carbon nanotube (CNT)/TiO_2 coaxial nanocables, which demonstrate that two intimately connected phases CNT and TiO_2, in fact, provide a clever solution to the ionic−electronic wiring problem in LIBs.[17] Graphene, a new two-dimensional (2D) carbon material,[18] was recently considered as a potential alternative for graphite in LIBs because of its superior electrical conductivity, high surface area of over 2600 m^2 g^{-1}, chemical tolerance, ultrathin thickness, and structural flexibility. Many types of hybrid materials consisting of graphene and electroactive materials have been successfully synthesized and used in LIBs to take advantage of their superior electrical conductivity and mechanical flexibility, such as SnO_2,[19−21] Fe_2O_3,[22] Fe_3O_4,[23−25] silicon,[26,27] Co_3O_4,[28,29] Sn,[30] $Li_4Ti_5O_{12}$,[31] TiO_2,[7,32] MnO_2,[33] and so forth. There is a fast electron transfer within a single graphene nanosheet, while the poor electronic contacts between graphene sheets (GNS) lower the overall conductivity of the resulting graphene-based composites. Also, the reduced graphite oxide (GO) easily forms irreversible agglomerates due to the $\pi-\pi$ interaction between individual GNS. The interesting performance of GNS is significantly lost due to the nanosheet aggregation, which is the most important issue for realizing the applications of GNS for electrode materials. One possible strategy to address the challenges mentioned above is to use one-dimensional (1D) CNTs to physically separate 2D graphene to preserve graphene's high surface area.[34,35]

Received: November 3, 2011
Accepted: November 28, 2011
Published: November 28, 2011

In this work, we report a solution-based method to synthesize a 3D TiO_2−GNS−CNT nanocomposite, in which the ultrathin anatase TiO_2 nanocrystalline is grown on 2D graphene and a 1D CNT. Long and tortuous CNTs not only bridge the defects for electron transfer between graphene layers underneath of TiO_2 nanomaterials but also could bridge adjacent GNS and inhibit their aggregation, resulting in a high contact area between the electrolyte/electrode and facilitating transportation of the electrolyte ion and electron into the inner region of the electrode. Specifically, this hybrid structure is able to deliver high reversible capacities and exhibit significantly enhanced cycling performance.

As shown in Figure 1, the pure TiO_2 synthesized by controlled hydrolysis of TBT exhibits good crystallinity and a

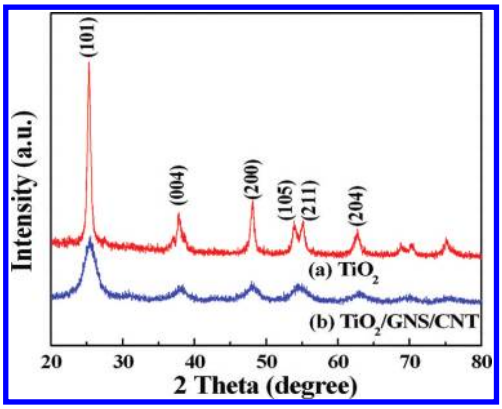

Figure 1. X-ray diffraction patterns of pristine TiO_2, and a 3D TiO_2−GNS−CNT nanocomposite.

typical anatase structure after annealing in N_2 at 400 °C, which is in accordance with those established by JCPDS card number 21-1272. The as-prepared 3D TiO_2−GNS−CNT nanocomposite retains the same position of the diffraction peaks of TiO_2. However, the broad and low diffraction peaks of TiO_2 in the TiO_2−GNS−CNT nanocomposite suggests a small crystallite size, which is consistent with the result from scanning electron microscope (SEM) images (Figure 2a,d). By using Scherrer's

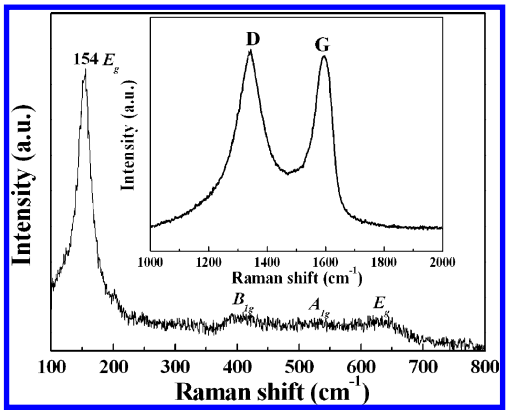

Figure 2. Raman spectra of the 3D TiO_2−GNS−CNT nanocomposite. The inset shows the D and G bands in the range of 1000−2000 cm^{-1}.

formula based on the (101) peak, the grain size of TiO_2 is estimated to be about 9 and 16 nm for pure TiO_2 and the TiO_2−GNS−CNT nanocomposite, respectively, which confirms that the GNS−CNT prevents the TiO_2 particle from coalescence during the calcination process.

The chemical composition of the TiO_2−GNS−CNT nanocomposite was also confirmed by Raman spectroscopy, as seen in Figure 2. A well-resolved TiO_2 Raman peak is clearly seen at about 153 cm^{-1}, which is attributed to the main E_g anatase vibration mode, against 144 cm^{-1} of bare TiO_2. The shift toward high frequency is caused by the interaction of TiO_2 with graphene.[36] Furthermore, vibration peaks at about 400 (B_{1g}), 516 (A_{1g}), and 639 cm^{-1} (E_g) are also characteristic of anatase TiO_2.[37] The Raman spectra are therefore consistent with the XRD results shown in Figure 1. Additionally, two broad peaks displayed at about 1334 and 1596 cm^{-1} are observed in the spectra (see the inset in Figure 2), which can be assigned to the D and G peaks of the graphene substrate. A stronger D band was observed than G band, indicating a largely disordered structure of the obtained GNS.

Figure 3 displays the FESEM images of the pristine TiO_2, GNS−CNT, and 3D TiO_2−GNS−CNT nanocomposite. In

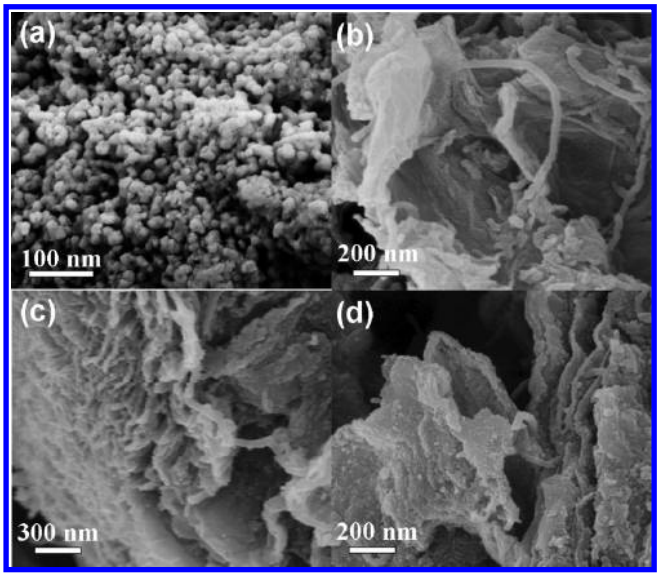

Figure 3. SEM images of (a) TiO_2 nanoparticles, (b) GNS−CNT, and (c,d) a 3D TiO_2−GNS−CNT nanocomposite.

Figure 3a, the product prepared in the absence of the GO−CNT consisted of only irregular nanoparticle aggregates with the size of 12−20 nm. Figure 3b shows the SEM image of the GNS−CNT composite; CNTs are uniformly dispersed and bonded to the graphene surface as well as embedded in the graphene sheets. When TBT and some water were added into the GO−CNT hybrid dispersion, TiO_2 nanoparticles homogeneously anchored on graphene layers, avoiding/weakening the loss of their high active surface area. SEM images in Figure 3c,d clearly show uniform TiO_2 nanoparticles and CNTs not only on the surface of the stacked structure but also between the parallel layers of the graphene, which act as pillars to effectively separate the graphene sheets from each other, leading to a porous and loose architecture. GNS are used as support materials for deposition of TiO_2 nanoparticles, and CNTs used as conductive wires could be expected to connect each p-conjugation structure of the TiO_2-decorated graphene sheets; such a structure would serve to further improve the conductivity of the composite.

To further examine the architecture of the composite, the samples were investigated by transmission electron microscopy (TEM). Figure 4a presents the typical TEM micrographs of the

dx.doi.org/10.1021/jz201456p | J. Phys. Chem.Lett. 2011, 2, 3096−3101

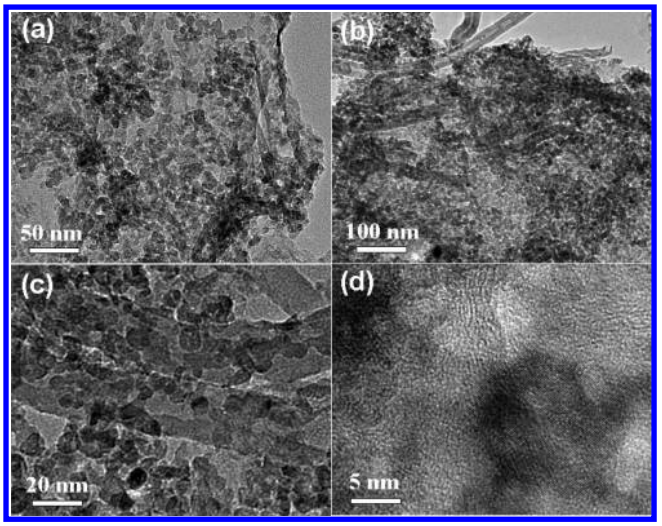

Figure 4. TEM images of (a) TiO_2–GNS and (b–d) a 3D TiO_2–GNS–CNT nanocomposite.

TiO_2–GNS mixtures, in which TiO_2 nanoparticles were attached on the graphene surface. The image shown in Figure 4b reveals that the individual CNTs are dispersed on the graphene surface and/or embedded in the graphene sheets to form a 3D hierarchical structure, indicating successful incorporation of CNTs onto the graphene sheets. TiO_2 nanoparticles are uniformity attached on the GNS and CNT surface, and their average particle size is in the range of 8–10 nm (Figure 4c,d). Therefore, GNS stacking is significantly reduced by constructing the GNS–CNT hierarchical structure, leading to higher porosity and larger specific surface area to enhance the electrochemical performances of 3D TiO_2–GNS–CNT. Also, the conductive CNT wraps around graphene/TiO_2 three-dimensionally to provide an additional electron-transport path besides the graphene layer underneath of TiO_2 nanomaterials, greatly enhancing their lithium ion storage capacity.

On the basis of the nanostructural observations made from the above SEM and TEM images, the overall fabrication procedures of the 3D TiO_2–GNS–CNT nanocomposite are schematically illustrated in Figure 5. We treated as-received CNTs with strong nitric acid to create functional oxygenated groups on their surfaces. Acid-treated carbon nanotubes can be well dispersed in ethanol, and the individual CNTs are adsorbed onto the surface of GO sheets due to the p-stacking interactions. The 3D GO–CNT matrix with a high density of functional groups is the key factor in controlling the morphology by acting as the nucleation site for deposits through interaction with metal. Three-dimensional structure might be expected to increase the area of the surface available for anchoring TiO_2 particles. TBT is added into the GO–CNT hybrid dispersion to form a homogeneous suspension through interaction of the metal ions with oxygen-containing functional groups. After adding some water into the ethanol solution under magnetic stirring, uniform-sized TiO_2 nanoparticles are formed in situ and attached onto the surface of GO nanosheets and CNTs. Finally, GO nanosheets are reduced to a highly conductive form of graphene using hydrazine hydrate as the reductant followed by a thermal treatment. During this process, CNTs on graphene reduce the π–π interaction between graphene sheets resulting from steric hindrance, thereby preventing aggregation, leaving in abundant pores in the 3D hierarchical structure. This unique hybrid structure is advantageous for the electrochemical performance of lithium ion batteries because the CNT can bridge the nanocrystalline TiO_2-decorated GNS to form an effective conducting network and enhance ion diffusion kinetics.

The porous structure and Brunauer–Emmett–Teller (BET) specific surface area of pure TiO_2 particles, TiO_2–GNS, and 3D TiO_2–GNS–CNT nanocomposites were investigated by nitrogen isothermal adsorption. As shown in Figure 6, the nitrogen adsorption–desorption isotherm with the distinct hysteresis loops can be attributed to type IV, according to IUPAC classification. As summarized in Table 1, the BET surface area and the pore volume of TiO_2 were significantly increased after the incorporation of GNS, namely, from 34.2 to 263.5 $m^2\ g^{-1}$ and from 0.054 to 0.219 $cm^3\ g^{-1}$, respectively. After the introduction of CNT, the 3D TiO_2–GNS–CNT

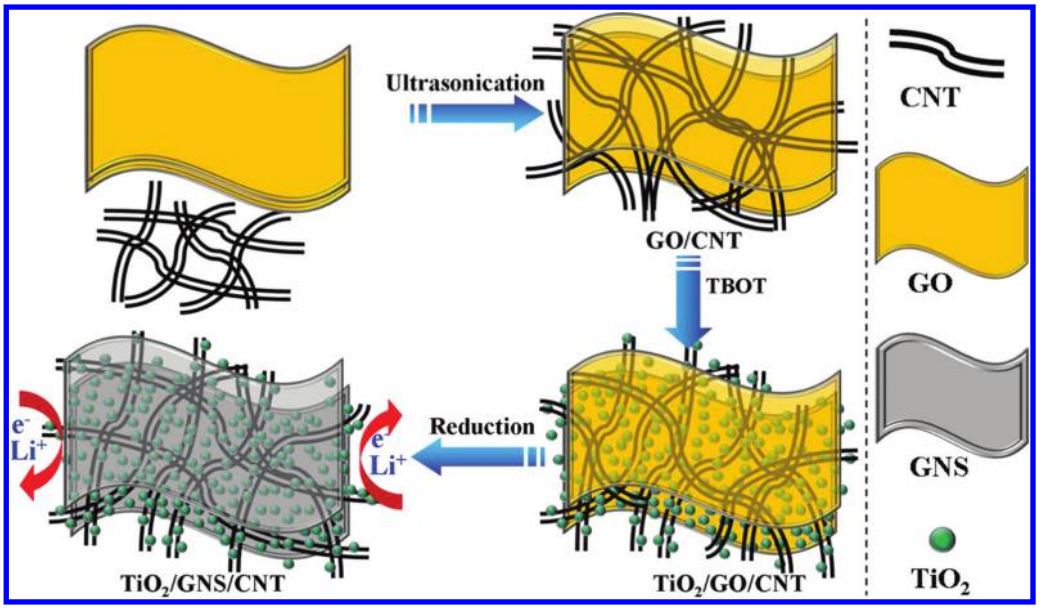

Figure 5. Schematic illustration for the synthesis of 3D TiO_2–GNS–CNT nanocomposites.

dx.doi.org/10.1021/jz201456p | J. Phys. Chem.Lett. 2011, 2, 3096–3101

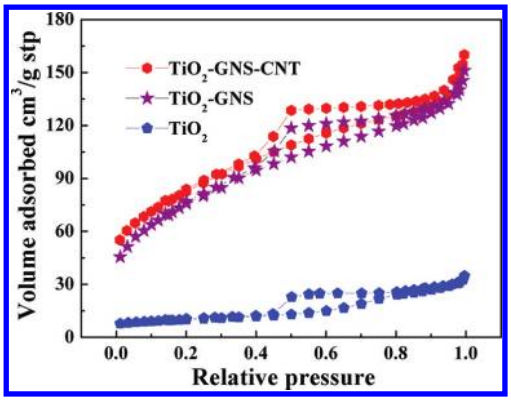

Figure 6. Nitrogen adsorption−desorption isotherm curves of TiO_2, TiO_2−GNS, and TiO_2−GNS−CNT nanocomposites.

Table 1. BET Surface Area and Pore Volume of TiO_2 and TiO_2−GNS−CNT Nanocomposites

sample	S_{BET} (m^2 g^{-1})	pore volume (cm^3 g^{-1})
TiO_2	34.2	0.054
TiO_2−GNS	263.5	0.219
TiO_2−GNS−CNT	291.2	0.248

nanocomposite exhibited higher specific surface area (291.2 m^2 g^{-1}) and larger pore volume (0.248 cm^3 g^{-1}), which should be attributed to the rigid CNT effectively preventing the restacking of flexible GNS to increase the basal spacing. On the basis of the Barrett−Joyner−Halenda (BJH) equation, the main pore size (Figure S1, Supporting Information) in the TiO_2−GNS−CNT nanocomposite is 3.9 nm, which is smaller than that for bare TiO_2 nanoparticles (6.4 nm). The relatively large surface area provided by the TiO_2−GNS−CNT nanocomposite would increase the electrolyte/electrode contact area, which would lead to a decrease of the current density per unit surface area and an increase in the charge/discharge rate.

The electrochemical properties of 3D TiO_2−GNS−CNT, TiO_2−GNS, and pure TiO_2 were evaluated and compared (Figure 7). Figure 7a shows the charge/discharge voltage profiles of the three samples at a current rate of 1 C between 1.0 and 3.0 V. It is evident that the discharge process of the three samples consists of three stages; the first stage is the quick voltage drop, the second stage is the distinct voltage plateau, and the third stage is a gradual decay in potential. The plateaus are related to the phase transition between the tetragonal and orthorhombic phases with Li insertion into anatase TiO_2.[15] Apparently, TiO_2−GNS−CNT is able to deliver a larger discharge capacity of 163.7 mA h g^{-1}, while the TiO_2−GNS and pure TiO_2 exhibit a lower discharge capacity, 155.4 and 141.3 mA h g^{-1}, respectively. Also, the voltage profiles of the pure TiO_2 and TiO_2−GNS exhibited a relatively higher charging plateau and lower discharging plateau compared to the TiO_2−GNS−CNT hybrid, which is mainly related to the high electrode polarization.[38]

The rate performances of TiO_2−GNS−CNT, TiO_2−GNS, and TiO_2 nanoparticles at the current rates of 0.5−30 C are compared in Figure 7b. Remarkably, as the discharge/charge rate increased from 0.5 to 30 C, the discharge capacities of pure TiO_2 decreased steeply, whereas the TiO_2−GNS mixture decreased relatively slower at the same rate. By introducing conductive CNT wraps around TiO_2−GNS to form a 3D hierarchical structure, TiO_2−GNS−CNT hybrid nanostructures exhibited the highest rate capacity among the three samples. It is noteworthy that the capacity (93.1 mA h g^{-1}) obtained by TiO_2−GNS−CNT nanocomposite at a rate of 30 C is higher than that obtained at a rate of 10 C for the pure TiO_2 and 20 C for the TiO_2−GNS mixture. TiO_2−GNS−CNT hybrid nanostructures have better electrochemical properties than graphene-wrapped TiO_2 hollow structures[15] and self-assembled TiO_2−graphene[7] but are similar to those of graphene−TiO_2 nanosheets with exposed (001) high-energy facets.[32] It was reported that the good electronic conductivity and nanosize particles may contribute to the high rate discharge performance. To confirm the improved electronic conductivity after introducing CNTs into a TiO_2−GNS composite, we measured the electronic conductivity of the TiO_2, TiO_2−GNS, and TiO_2−GNS−CNT nanocomposites. The TiO_2−GNS−CNT nanocomposites reveal a significant increase in electronic conductivity (ca. 0.087 S cm^{-1}), as compared with that of TiO_2 nanoparticles (ca. 10^{-6} S cm^{-1}) and TiO_2−GNS composites (ca. 0.0012 S cm^{-1}), demonstrating that CNTs play an important role in enhancing the conductivity of the composite.

The cycling behaviors for the three different samples at the rate of 10 C are shown in Figure 7c. The discharge capacity in the first cycle of the TiO_2−GNS−CNT nanocomposite was 121.8 mA h g^{-1} at the rate of 10 C, after 100 cycles with 8.7% capacity loss, but for TiO_2−GNS and pristine TiO_2, the corresponding values were 103.4 mA h g^{-1} and 11.5% and 72.3 mA h g^{-1} and 14.7% respectively. This result demonstrates that the TiO_2−GNS−CNT nanocomposite with a 3D hierarchical structure is very stable, and the electrochemical Li^+ insertion/extraction process is quite reversible even at high rates. The improved high rate performance and cycling ability may be attributed to three aspects. (1) CNTs as conductive wires connect each TiO_2-decorated graphene sheets, and such

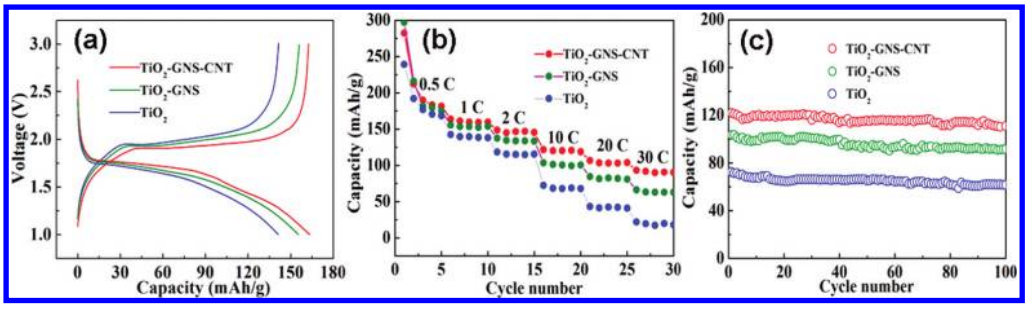

Figure 7. (a) Charge/discharge voltage profiles of pure TiO_2, TiO_2−GNS, and the TiO_2−GNS−CNT nanocomposite at a rate of 1 C. (b) Rate performance of pure TiO_2, TiO_2−GNS, and the TiO_2−GNS−CNT nanocomposite electrodes at different current rates. (c) Cycling performance of the three different samples at a current rate of 10 C.

dx.doi.org/10.1021/jz201456p | J. Phys. Chem.Lett. 2011, 2, 3096−3101

structure would serve to further improve the conductivity of the composite. (2) The CNT attached on the surface of graphene reduces the $\pi-\pi$ interaction between graphene sheets resulting from steric hindrance, resulting in reducing the degree of restacking of GNS and consequently keeping their large active contact area between the electrode and electrolyte, which leads to a decrease of the current density per unit surface area and an increase in the charge/discharge rate. (3) The hierarchical GNS−CNT architecture could provide a support for anchoring well-dispersed TiO_2, which hinders TiO_2 nanoparticle agglomeration and growth during the calcination process and thus reduces the transport path lengths of lithium ions and electrons.

In summary, we have developed a facile route to synthesize 3D TiO_2−GNS−CNT nanocomposites as an advanced anode material for high-power LIBs. The TiO_2 nanoparticles were uniformly dispersed on the surface of graphene and carbon nanotubes, which serve as the ideal host for fast and efficient lithium storage. The interlaced carbon nanotubes were intimately embedded or attached on the graphene to form highly conductive 3D networks, which serves as a highly conductive substrate that is beneficial to the high-rate performance. At the same time, the large surface area provides more reaction sites and lower activation energy for lithium ion insertion/deinsertion. It is believed that such 3D hybrid materials composed of nanoactive particles (0D), carbon nanotubes (1D), and graphene (2D) with designed structure and varied properties will be useful in energy storage and other important applications.

■ ASSOCIATED CONTENT

Ⓢ Supporting Information

Experimental details and pore size distribution patterns (Figure S1). This material is available free of charge via the Internet at http://pubs.acs.org.

■ AUTHOR INFORMATION

Corresponding Author

*E-mail: azhangxg@nuaa.edu.cn. Tel: +86-25-52112918. Fax: +86-25-52112626.

■ ACKNOWLEDGMENTS

This work was supported by the National Natural Science Foundation of China (No. 20873064, 21173120), Specialized Research Fund for the Doctoral Program of Higher Education of China (No. 20060287026), Natural Science Foundation of Jiangsu Province (No. BK2011030), Jiangsu Innovation Program for Graduate Education (CXZZ11_0204), and Outstanding Doctoral Dissertation in NUAA (BCXJ11-10). L.S. would also like to thank the China Scholarship Council (CSC) for providing his exchange scholarship for Ph.D. study at the University of Washington.

■ REFERENCES

(1) Kubiak, P.; Fröschl, T.; Hüsing, N.; Hörmann, U.; Kaiser, U.; Schiller, R.; K. Weiss, C.; Landfester, K.; Wohlfahrt-Mehrens, M. TiO_2 Anatase Nanoparticle Networks: Synthesis, Structure, and Electrochemical Performance. *Small* **2011**, *7*, 1690−1696.

(2) McCloskey, B.; Luntz, A. C.; Swanson, S.; Wilcke, W. Lithium−Air Battery: Promise and Challenges. *J. Phys. Chem. Lett.* **2010**, *1*, 2193−2203.

(3) Manthiram, A. Materials Challenges and Opportunities of Lithium Ion Batteries. *J. Phys. Chem. Lett.* **2011**, *2*, 176−184.

(4) Aricò1, A. S.; Bruce, P.; Scrosati, B.; Tarascon, J. M.; Schalkwijk, W. V. Nanostructured Materials for Advanced Energy Conversion and Storage Devices. *Nat. Mater.* **2005**, *4*, 366−377.

(5) Shen, L. F.; Yuan, C. Z.; Luo, H. J.; Zhang, X. G.; Xu, K.; Xia, Y. Y. Facile Synthesis of Hierarchically Porous $Li_4Ti_5O_{12}$ Microspheres for High Rate Lithium Ion Batteries. *J. Mater. Chem.* **2010**, *20*, 6998−7004.

(6) Chen, J. S.; Tan, Y. L.; Li, C. M.; Cheah, Y. L.; Luan, D. Y.; Madhavi, S.; Boey, F. Y. C.; Archer, L. A.; Lou, X. W. Constructing Hierarchical Spheres from Large Ultrathin Anatase TiO_2 Nanosheets with Nearly 100% Exposed (001) Facets for Fast Reversible Lithium Storage. *J. Am. Chem. Soc.* **2010**, *132*, 6124−6130.

(7) Wang, D. H.; Choi, D. W.; Li, J.; Yang, Z. G.; Nie, Z. M.; Kou, R.; Hu, D. H.; Wang, C. M.; Saraf, L. V.; Zhang, J. G.; Aksay, I. A.; Liu, J. Self-Assembled TiO_2−Graphene Hybrid Nanostructures for Enhanced Li-Ion Insertion. *ACS Nano* **2009**, *3*, 907−914.

(8) Guo, Y. G.; Hu, Y. S.; Sigle, W.; Maier, J. Superior Electrode Performance of Nanostructured Mesoporous TiO_2 (Anatase) Through Efficient Hierarchical Mixed Conducting Networks. *Adv. Mater.* **2007**, *19*, 2087−2091.

(9) Wang, D. H.; Choi, D. W.; Yang, Z. G.; Viswanathan, V. V.; Nie, Z. M.; Wang, C. G.; Song, Y. J.; Zhang, J. G.; Liu, J. Synthesis and Li-Ion Insertion Properties of Highly Crystalline Mesoporous Rutile TiO_2. *Chem. Mater.* **2008**, *20*, 3435−3442.

(10) Pol, V. G.; Kang, S. H.; Calderon-Moreno, J. M.; Johnson, C. S.; Thackeray, M. M. Autogenic Reactions for Preparing Carbon-Encapsulated, Nanoparticulate TiO_2 Electrodes for Lithium-Lon Batteries. *J. Power Sources* **2010**, *195*, 5039−5043.

(11) Kim, H.; Kim, M. G.; Shin, T. J.; Shin, H. J.; Cho, J. TiO_2@Sn Core−Shell Nanotubes for Fast and High Density Li-Ion Storage Material. *Electrochem. Commun.* **2008**, *10*, 1669−1672.

(12) Chen, J. S.; Liu, H.; Qiao, S. Z.; Lou, X. W. Carbon-Supported Ultra-Thin Anatase TiO_2 Nanosheets for Fast Reversible Lithium Storage. *J. Mater. Chem.* **2011**, *21*, 5687−5692.

(13) Jung, H. G.; Oh, S. W.; Ce, J.; Jayaprakash, N.; Sun, Y. K. Mesoporous TiO_2 Nano Networks: Anode for Nigh Power Lithium Battery Applications. *Electrochem. Commun.* **2009**, *11*, 756−759.

(14) Das, S. K.; Darmakolla, S.; Bhattacharyya, A. J. High Lithium Storage in Micrometre Sized Mesoporous Spherical Self-Assembly of Anatase Titania Nanospheres and Carbon. *J. Mater. Chem.* **2010**, *20*, 1600−1606.

(15) Chen, J. S.; Wang, Z. Y.; Dong, X. C.; Chen, P.; Lou, X. W. Graphene-Wrapped TiO_2 Hollow Structures with Enhanced Lithium Storage Capabilities. *Nanoscale* **2011**, *3*, 2158−2161.

(16) Shen, L. F.; Yuan, C. Z.; Luo, H. J.; Zhang, X. G.; Chen, L.; Li, H. S. Novel Template-Free Solvothermal Synthesis of Mesoporous $Li_4Ti_5O_{12}$−C Microspheres for High Power Lithium Ion Batteries. *J. Mater. Chem.* **2011**, *21*, 14414−14416.

(17) Cao, F. F.; Guo, Y. G.; Zheng, S. F.; Wu, X. L.; Jiang, L. Y.; Bi, R. R.; Wan, L. J.; Maier, J. Symbiotic Coaxial Nanocables: Facile Synthesis and an Efficient and Elegant Morphological Solution to the Lithium Storage Problem. *Chem. Mater.* **2010**, *22*, 1908−1914.

(18) Geim, A. K.; Novoselov, K. S. The Rise of Graphene. *Nat. Mater.* **2007**, *6*, 183−191.

(19) Paek, S. M.; Yoo, E.; Honma, I. Enhanced Cyclic Performance and Lithium Storage Capacity of SnO_2/Graphene Nanoporous Electrodes with Three-Dimensionally Delaminated Flexible Structure. *Nano Lett.* **2009**, *9*, 72−75.

(20) Ding, S. J.; Luan, D. Y.; Boey, F. Y. C.; Chen, J. S.; Lou, X. W. SnO_2 Nanosheets Grown on Graphene Sheets with Enhanced Lithium Storage Properties. *Chem. Commun.* **2011**, *47*, 7155−7157.

(21) Li, Y. M.; Lv, X. J.; Lu, J.; Li, J. H. Preparation of SnO_2-Nanocrystal/Graphene-Nanosheets Composites and Their Lithium Storage Ability. *J. Phys. Chem. C* **2010**, *114*, 21770−21774.

(22) Zhu, X. J.; Zhu, Y. W.; Murali, S.; Stoller, M. D.; Ruoff., R. S. Nanostructured Reduced Graphene Oxide/Fe_2O_3 Composite as a High-Performance Anode Material for Lithium Ion Batteries. *ACS Nano* **2011**, *5*, 3333−3338.

(23) Zhang, M.; Lei, D. N.; Yin, X. M.; Chen, L. B.; Li, Q. H.; Wang, Y. G.; Wang., T. H. Magnetite/Graphene Composites: Microwave

Irradiation Synthesis and Enhanced Cycling and Rate Performances for Lithium Ion Batteries. *J. Mater. Chem.* **2010**, *20*, 5538−5543.
(24) Zhou, G. M.; Wang, D. W.; Li, F.; Zhang, L. L.; Li, N.; Wu, Z. S.; Wen, L.; Lu, G. Q.; Cheng, H. M. Graphene-Wrapped Fe_3O_4 Anode Material With Improved Reversible Capacity and Cyclic Stability for Lithium Ion Batteries. *Chem. Mater.* **2010**, *22*, 5306−5313.
(25) Wang, J. Z.; Zhong, C.; Wexler, D.; Idris, N. H.; Wang, Z. X.; Chen, L. Q.; Liu., H. K. Graphene-Encapsulated Fe_3O_4 Nanoparticles with 3D Laminated Structure as Superior Anode in Lithium Ion Batteries. *Chem.—Eur. J.* **2011**, *17*, 661−667.
(26) Lee, J. K.; Smith, K. B.; Hayner, C. M.; Kung, H. H. Silicon Nanoparticles−Graphene Paper Composites for Li Ion Battery Anodes. *Chem. Commun.* **2010**, *46*, 2025−2027.
(27) Chou, S. L.; Wang, J. Z.; Choucair, M.; Liu, H. K.; Stride, J. A.; Dou, S. X. Enhanced Reversible Lithium Storage in Nanosize Silicon/Graphene Composite. *Electrochem. Commun.* **2010**, *12*, 303−306.
(28) Wang, B.; Wang, Y.; Park, J.; Ahn, H.; Wang, G. X. *In situ* Synthesis of Co_3O_4/Graphene Nanocomposite Material for Lithium-Ion Batteries and Supercapacitors with High Capacity and Supercapacitance. *J. Alloys Compd.* **2011**, *509*, 7778−7783.
(29) Chen, S. Q.; Wang, Y. Microwave-Assisted Synthesis of a Co_3O_4−Graphene Sheet-on-Sheet Nanocomposite as a Superior Anode Material for Li-Ion Batteries. *J. Mater. Chem.* **2010**, *20*, 9735−9739.
(30) Wang, G. X.; Wang, B.; Wang, X. l.; Park, J.; Dou, S. X.; Ahn, H.; Kim., K. Sn/Graphene Nanocomposite with 3D Architecture for Enhanced Reversible Lithium Storage in Lithium Ion Batteries. *J. Mater. Chem.* **2009**, *19*, 8378−8384.
(31) Shen, L. F.; Yuan, C. Z.; Luo, H. J.; Zhang, X. G.; Yang, S. D.; Lu, X. J. *In Situ* Synthesis of High−Loading $Li_4Ti_5O_{12}$−Graphene Hybrid Nanostructures for High Rate Lithium Ion Batteries. *Nanoscale* **2011**, *3*, 572−574.
(32) Ding, S. J.; Chen, J. S.; Luan, D. Y.; Boey, F. Y. C.; Madhavibc, S.; Lou, X. W. Graphene-Supported Anatase TiO_2 Nanosheets for Fast Lithium Storage. *Chem. Commun.* **2011**, *47*, 5780−5782.
(33) Yu, A. P.; Park, H. W.; Davies, A.; Higgins, D. C.; Chen, Z. W.; Xiao, X. C. Free-Standing Layer-by-Layer Hybrid Thin Film of Graphene−MnO_2 Nanotube as Anode for Lithium Ion Batteries. *J. Phys. Chem. Lett.* **2011**, *2*, 1855−1860.
(34) Novaes, F. D.; Rurali, R.; Ordejon, P. Electronic Transport Between Graphene Layers Covalently Connected by Carbon Nanotubes. *ACS Nano* **2010**, *4*, 7596−7602.
(35) Yu, D. S.; Dai, L. M. Self-Assembled Graphene/Carbon Nanotube Hybrid Films for Supercapacitors. *J. Phys. Chem. Lett.* **2010**, *1*, 467−470.
(36) Li, N.; Liu, G.; Zhen, C.; Li, F.; Zhang, L. L.; Cheng, H. M. Battery Performance and Photocatalytic Activity of Mesoporous Anatase TiO_2 Nanospheres/Graphene Composites by Template-Free Self-Assembly. *Adv. Funct. Mater.* **2011**, *21*, 1717−1722.
(37) Zhang, H. L.; Xu, P. P.; Du, G. D.; Chen, Z. W.; Oh, K.; Pan, D. Y.; Jiao., Z. A Facile One-Step Synthesis of TiO_2/Graphene Composites for Photodegradation of Methyl Orange. *Nano Res.* **2011**, *4*, 274−283.
(38) Shen, L. F.; Yuan, C. Z.; Luo, H. J.; Zhang, X. G.; Xu, K.; Zhang, F. In Situ Growth of $Li_4Ti_5O_{12}$ on Multi-Walled Carbon Nanotubes: Novel Coaxial Nanocables for High Rate Lithium Ion Batteries. *J. Mater. Chem.* **2011**, *21*, 761−767.